Importance of Accurate Liquid Water Path for Estimation of Solar Radiation in Warm Boundary Layer Clouds: An Observational Study

MANAJIT SENGUPTA

Pacific Northwest National Laboratory, Richland, Washington

EUGENE E. CLOTHIAUX

The Pennsylvania State University, University Park, Pennsylvania

THOMAS P. ACKERMAN

Pacific Northwest National Laboratory, Richland, Washington

SEIJI KATO

Center for Atmospheric Sciences, Hampton University, Hampton, Virginia

QILONG MIN

Atmospheric Sciences Research Center, State University of New York at Albany, Albany, New York

(Manuscript received 7 October 2002, in final form 17 February 2003)

ABSTRACT

A 1-yr observational study of overcast boundary layer stratus at the U.S. Department of Energy Atmospheric Radiation Measurement Program Southern Great Plains site illustrates that surface radiation has a higher sensitivity to cloud liquid water path variations when compared to cloud drop effective radius variations. The mean, median, and standard deviation of observed cloud liquid water path and cloud drop effective radius are 0.120, 0.101, 0.108 mm and 7.38, 7.13, 2.39 μm, respectively. Liquid water path variations can therefore cause 3 times the variation in optical depth as effective radius—a direct consequence of the comparative variability displayed by the statistics of the two parameters. Radiative transfer calculations demonstrate that, over and above the impact of higher liquid water path variability on optical depth, normalized cloud forcing is 2 times as sensitive to liquid water path variations as it is to effective radius variations. Consequently, radiative transfer calculations of surface flux using observed liquid water paths and a fixed effective radius of 7.5 μm have a 79% correlation with observed values. This higher sensitivity of solar flux to liquid water path is a result of the regimes of natural occurrence of cloud liquid water paths and cloud drop effective radii.

1. Introduction

Low-level water clouds, including stratocumulus and stratus, cover 34% of the ocean and 18% of the land at any given time (Heymsfield 1993). These clouds normally have a high albedo when compared to land and ocean surfaces with temperatures that are comparable to them. Consequently, low stratiform clouds provide about 60% of the annually averaged net cloud radiative forcing at the top of the atmosphere (Hartmann et al. 1992). Two quantities used to quantify the radiative impact of these clouds are the cloud particle effective radius and the cloud liquid water path (Stephens 1978; Hu and Stamnes 1993). Numerous studies (e.g., Charlson et al. 1987; Han et al. 1994; Ramaswamy and Chen 1993; Chen and Ramaswamy 1996; Szczodrak et al. 2001) have tried to assess the impact of individual variations in these parameters on radiative forcing and climate feedback.

Most studies of this type are satellite based, and assessment of simultaneous variations in the two parameters and the capacity of one to offset changes in the other within natural limits is difficult to gauge with data having coarse spatial resolution. Aircraft-based measurements (Albrecht et al. 1995; Duda et al. 1991; Martin et al. 1994; Noonkester 1984), although complementary to satellite data, result in small temporal sam-

Corresponding author address: Manajit Sengupta, Pacific Northwest National Lab., 3200-Q Avenue MSIN K9-24, Richland, WA 99352.
E-mail: manajit@pnl.gov

ples that preclude climatological assessments. Surface-based remote sensors, however, are capable of providing continuous data at a much smaller cost than aircraft-based measurements. Therefore, we use measurements from a variety of remote sensing instruments located at the central facility of the U.S. Department of Energy (DOE) Atmospheric Radiation Measurement (ARM) Program Southern Great Plains (SGP) site in Oklahoma (36.605°N, 97.485°W) to intensively study the radiative effects of warm boundary layer clouds.

To quantify the radiative properties of boundary layer clouds we require information regarding a minimum of two parameters: liquid water path and effective radius. While the clouds are detectable using radars and lidars, or a combination of both, inferring the size distributions of cloud droplets is a complex task. Possible methods involve the use of radar reflectivities (Kato et al. 2001) or surface radiation measurements (Min and Harrison 1996) along with the column liquid water path retrieved from a microwave radiometer (Liljegren et al. 2001) as a constraint.

Ackerman et al. (1999) developed a paradigm for assessing the accuracy of parameterizations and retrievals of cloud microphysics from a radiative transfer perspective. The paradigm involves calculating surface solar fluxes using cloud microphysics from different sources and comparing the results with actual radiation measurements. We adapt the paradigm to assess retrievals of boundary layer cloud liquid water paths and cloud drop effective radii. A best-fit baseline effective radius appropriate for stratus at the ARM SGP site is used for comparison. We also assess the sensitivity of surface flux to each of the two parameters that we used to describe the radiative properties of boundary layer clouds.

2. Methodology

Our study depends upon accurate radiative transfer calculations through low-altitude liquid water clouds, which in turn depend upon accurate model treatments of absorption, scattering, and the atmospheric state. In this section we describe the radiative transfer model and its required input parameters, as well as the measurements of the atmospheric state, their availability, and their limitations.

a. The radiative transfer model

The one-dimensional radiative transfer model used in this study is based on the delta two-stream numerical algorithm presented by Toon et al. (1989) and Kato et al. (1999a), known as the Rapid Radiative Transfer (RAPRAD) model. The model has 32 spectral intervals ranging from 0.24 to 4.6 μm in the shortwave and near-infrared, using absorption coefficients based on k distributions and a correlated-k approximation (Kato et al. 1999b). The top-of-the-atmosphere solar spectral irradiance in the RAPRAD model is based on the solar irradiance of the moderate resolution transmittance (MODTRAN3) code (Berk et al. 1989). The RAPRAD model incorporates ozone, oxygen, carbon dioxide, and water vapor absorption, as well as water vapor continuum absorption. The molecular scattering optical depth is computed using the Rayleigh optical depth calculation from Hansen and Travis (1974).

The atmospheric layers in the RAPRAD model are user specified. We set the top of the atmosphere at 70 km and divided the atmosphere below 16 km into 250-m-thick layers. Above 16 km, model layer thicknesses increased with altitude. Clouds can be represented by additional layers in order to handle in-cloud variation of properties. Clouds within a layer are then modeled as homogeneous, with cloud properties allowed to vary from one layer to the next. In the model simulations we used a surface albedo of 0.2 that was invariant with wavelength; this value is typical of the surface albedo at the SGP site in the midvisible spectral range. It may be noted that spectrally varying albedo was found to have negligible impact on downwelling surface fluxes.

Clear-sky RAPRAD irradiance calculations require vertical profiles of pressure, temperature, water vapor, ozone, and aerosol particles. When a cloud is inserted into the RAPRAD model, cloud optical depth is a required input, together with the asymmetry parameter and single-scattering albedo of the cloud particles for each model wavelength interval.

Clear-sky flux calculations by Kato et al. (1997) that used SGP site atmospheric state measurements in the RAPRAD model exceeded measurements by approximately 35 W m^{-2}. Long et al. (2001) later found that infrared energy loss from the Eppley Precision Spectral Pyranometers (PSP) led to underestimates in measured diffuse irradiance of approximately 15 W m^{-2} in clear-sky conditions. Charlock et al. (2001) subsequently found a clear-sky surface flux bias of around -2 W m^{-2} when comparing radiative transfer calculations to Eppley Black and White pyranometer measurements, which do not suffer problems from infrared energy loss. Since then, Ackerman et al. (2003) have shown that uncertainties in aerosol properties can result in a 15–20 W m^{-2} uncertainty in RAPRAD calculations when compared to similar Eppley Black and White pyranometer measurements. Our use of uncorrected surface flux measurements from Eppley PSP instruments can, therefore, lead to a maximum overestimate comparable to Kato et al. (1997).

b. Measurements of atmospheric state at the SGP site

In Table 1 we match the required inputs of the RAPRAD model with the instruments at the SGP site that are providing them. An accurate vertical profile of the atmospheric thermodynamic state, especially of the vertical distribution of water vapor, is important for a reliable computation of broadband irradiance at the surface. At the SGP site multiple sets of measurements are

TABLE 1. Summary of atmospheric variables, their source of measurement, and the resolution at which they are available.

Variables	Source	Time resolution
Cloud boundaries	Millimeter-Wave Cloud Radar (MMCR)	10 s
	Micropulse Lidar (MPL)	
	Belfort Ceilometer (BLC)	
	Atmospheric Remote Sensing of Clouds (ARSCL) data	
Liquid water path	Microwave Radiometer (MWR)	20 s
Water vapor column	MWR	20 s
Temperature profile	Balloonborne Sounding System (BBSS)	1 min
Pressure profile	Atmospheric Emitted Radiance Interferometer (AERI)	
Mixing ratio profile	RUC*	
	MWR	
	Surface Meteorological Observation System (SMOS)	
Aerosol optical depth	Multi-Filter Rotating Shadowband Radiometer (MFRSR)	30 min
	Total ozone monitoring satellite (TOMS)	
Effective radius (Kato et al. 2001)	MMCR	20 s
	MWR	
Effective radius (Min and Harrison 1996)	MFRSR	5 min
	MWR	

* Rapid Update Cycle (RUC) weather forecast model from NOAA Forecast System Laboratory.

used to construct atmospheric profiles with the highest possible temporal resolution. Radiosonde data are used to scale vertically integrated measurements of water vapor retrieved either from a microwave radiometer (Liljegren 1994) or a combination of interferometer and Geostationary Operational Environmental Satellite (GOES) satellite radiance measurements across the thermal infrared (Schmit et al. 2002). For those periods when ground-based observations are not available, thermodynamic state profiles from numerical weather prediction models forced by observations are used. Surface meteorological stations provide high temporal resolution measurements of surface pressure, temperature, and moisture.

The Multi-Filter Rotating Shadowband Radiometer (MFRSR; Harrison et al. 1994) provides continuous measurements of direct normal solar irradiance across six wavelength intervals, five of which are used to retrieve the corresponding atmospheric extinction optical depth (Michalsky et al. 2001). Aerosol optical depths retrieved at the five wavelengths are subsequently used to retrieve the parameters of the Angstrom relationship (Angstrom 1929). The asymmetry parameter and single-scattering albedo of aerosol particles, treated as spheres, are computed using the Toon and Ackerman (1981) Mie code. We used a mean radius of 0.58 μm and standard deviation of 1.35 μm (Kato et al. 1997) with refractive indices of mineral dust particles from d'Almeida et al. (1991).

Vertical distributions of cloud hydrometeors are retrieved from multiple active remote sensors consisting of a ceilometer, a micropulse lidar, and a millimeter-wavelength cloud radar (Clothiaux et al. 2000). Clouds are then classified based solely on temperature at their boundaries. To fulfill our warm boundary layer cloud criterion, cloud-base and cloud-top temperatures must be greater than 273 and 253 K, respectively. Two factors influence our selection of the minimum cloud-top temperature, one being the effect of restricting cloud thickness to a maximum of around 3 km based on a lapse rate of around 6 K km^{-1} and the other being a threshold where ice-nucleus concentrations are less than 1 L^{-1} (Hobbs 1993). We show later in our results that the actual cloud tops have temperatures well above the actual threshold. Moreover, in this study we only use boundary layer cloud cases with no overlying upper-level clouds.

Cloud liquid water paths are retrieved using a dual-channel microwave radiometer (Liljegren 1994). We use the retrieval developed by Liljegren et al. (2001) that incorporates information about the atmospheric state at each retrieval time step to reduce the retrieval uncertainty of the Westwater (1993) retrieval technique. The Westwater (1993) technique is known to produce liquid water paths during clear-sky periods (Del Genio and Wolf 2000). This problem is reduced substantially by using the new technique and we used the radar and lidar to determine the existence of cloud, thereby avoiding the problem completely.

c. *Microphysical and radiative properties of warm clouds*

Underlying all of the important microphysical and radiative properties of warm clouds is the warm cloud drop size distribution $n(r, z)$, where $n(r, z)$ is the density of cloud drops as a function of drop radius r and vertical height z in the atmosphere. Early research demonstrated that warm cloud drop size distributions are expected to be unimodal with a potentially long tail at larger sizes (Pruppacher and Klett 1997). For this reason cloud drop size distributions in remote sensing retrievals and recorded by in situ probes are generally parameterized using either a gamma or lognormal distribution, two distributions with long tails at larger particle sizes (Fla-

tau et al. 1989). Following Miles et al. (2000), we use a lognormal distribution in this study.

Early studies by Hansen and Travis (1974), Stephens et al. (1978), and Hu and Stamnes (1993) demonstrated that the radiative effects of warm clouds are well-characterized by the cloud liquid water path and the cloud particle effective radius r_e defined as the ratio of the third to second moments of the particle size distribution. If the clouds are treated as vertically homogeneous, the expression for the optical depth becomes

$$\tau(\lambda) = \sigma_{\text{ext}}(\lambda) N_t \Delta z, \tag{1}$$

where $\sigma_{\text{ext}}(\lambda)$ is the extinction cross section $\alpha_{\text{ext}}(r, \lambda)$ integrated across the drop size distribution, N_t is the number of cloud drops per unit volume, and Δz is the thickness of the cloud. In terms of the extinction efficiency

$$q_{\text{ext}}(r, \lambda) = \frac{\alpha_{\text{ext}}(r, \lambda)}{\pi r^2}, \tag{2}$$

and the cloud liquid water path LWP, the cloud optical depth becomes

$$\tau(\lambda) = \frac{3 Q_{\text{ext}}(\lambda) \text{LWP}}{4 \rho_w r_e}, \tag{3}$$

where $Q_{\text{ext}}(\lambda)$ is the extinction efficiency $q_{\text{ext}}(r, \lambda)$ integrated over the drop size distribution. Since $Q_{\text{ext}}(\lambda)$ asymptotes to 2 as particle sizes become much larger than the wavelength of the incident radiation and shortwave radiation generally contains wavelengths much smaller than the radii of cloud drops, we set $Q_{\text{ext}}(\lambda)$ equal to 2 in Eq. (3) to obtain

$$\tau = \frac{3 \text{LWP}}{2 \rho_w r_e}. \tag{4}$$

d. Retrieving the microphysical properties of clouds

Based on numerous in situ observations of warm clouds available in the literature, Miles et al. (2000) reported average values of 5.4 μm and 0.38 for the effective radius and logarithmic width, respectively, of continental boundary layer clouds. Comparing computed and observed downwelling surface fluxes, we first use a single effective radius in the calculations that reduces the bias between the entire observed and computed datasets, as opposed to each individual case, by adjusting the effective radius beginning with the Miles et al. (2000) value. We label this one value as the best-fit effective radius. This best-fit cloud drop effective radius is subsequently used to assess the performance of two boundary layer cloud drop effective radius retrievals that operate on the data streams available from the ARM SGP site.

The first retrieval, referred to as radar-based, by Kato et al. (2001) uses radar reflectivity and Doppler velocity from the millimeter-wavelength cloud radar, as well as cloud liquid water path estimated from a microwave radiometer, to infer the size distribution of boundary layer cloud particles. The value of effective radius so derived is independent of any measurement of surface radiation.

In addition to direct normal measurements, the MFRSR makes measurements of narrowband total and diffuse hemispheric downwelling surface irradiance at its six wavelengths. Min and Harrison (1996) use the 415-nm (nominal midpoint of an approximately 10-nm band) passband to estimate stratus cloud optical depth. They subsequently compute the effective radius, referred to as transmission based, using Eq. (4) and measurements of liquid water path provided by the microwave radiometer. We expect modeled values of broadband downwelling surface irradiance, based on the Min and Harrison (1996) cloud drop effective radius and cloud liquid water paths retrieved from microwave radiometer measurements, to produce close agreement with measurements as these radii were chosen to match the observed transmission in a visible solar band in the first place. Radar- and transmission-derived cloud drop effective radii are available for a 1-yr period extending from 1997 to 1998 and we use this time period for our study.

e. Comparing modeled and measured surface solar irradiance

To assess the reasonableness of retrieved cloud liquid water path and cloud drop effective radius we use them to compute downwelling broadband surface irradiances and we compare these irradiances with observations. A pyrheliometer provides observations of direct normal downwelling shortwave irradiance, while unshaded and shaded pyranometers measure the total and diffuse downwelling shortwave irradiances, respectively. In order to remove solar zenith angle effects in the comparisons, we opt to compare normalized cloud forcings instead of irradiances directly.

We define normalized cloud forcing as

$$\text{NCF}_c = \frac{f_c (F_{c,\text{cld}} - F_{c,\text{clr}})}{F_{c,\text{clr}}}, \tag{5}$$

where $F_{c,\text{cld}}$ is the computed downwelling surface shortwave irradiance during a cloudy period and $F_{c,\text{clr}}$ is what the computed downwelling surface shortwave irradiance would be if the sky were actually clear or free of clouds. The cloud fraction f_c weights the computed normalized cloud forcing in order to account for broken cloud sky conditions. In the case of observations the normalized cloud forcing is simply

$$\text{NCF}_o = \frac{F_{o,\text{cld}} - F_{o,\text{clr}}}{F_{o,\text{clr}}}, \tag{6}$$

where we have replaced the subscript ''c'' with an ''o'' and removed the explicit cloud fraction f_c since the

observed irradiance $F_{o,\mathrm{cld}}$ implicitly accounts for all sky conditions. As cloudy sky flux is less than clear-sky flux, apart from exceptional broken-cloud cases where the surface can receive an unattenuated direct beam radiation as well as diffuse radiation, the normalized cloud forcing lies between -1 and 0. In our study we chose cases with more than 90% cloud cover and therefore preclude cases with values above 0.

Computing normalized cloud forcing is straightforward, as producing a value of $F_{c,\mathrm{clr}}$ simply requires a radiative transfer calculation without any model clouds. However, obtaining values of observed normalized cloud forcing is more difficult, as one needs an estimate of the clear-sky irradiance $F_{o,\mathrm{clr}}$ that is based on observations during the same cloudy sky period. We use the method developed by Long and Ackerman (2000), which fits an empirical function to the measured downwelling shortwave irradiances for a day using all clear-sky periods during that day, to estimate $F_{o,\mathrm{clr}}$. On days with no clear-sky periods interpolation of the clear-sky function coefficients from surrounding days are used leading to a maximum uncertainty of 13 W m^{-2}, which is within actual measurement uncertainty (Long and Ackerman 2000).

f. Skill score assessment of modeled normalized cloud forcing

To assess how well modeled normalized cloud forcings match observed normalized cloud forcings we make use of the skill score developed by weather forecasters that is outlined in the appendix. In our implementation of the skill score, modeled normalized cloud forcings based on the best-fit effective radius are designated as the ''control.'' Modeled normalized cloud forcings obtained from the two sets of retrieved cloud drop effective radii are labeled as the ''forecast.'' By computing the mean square errors mse (see the appendix) between the control and observed data and each forecast dataset and observed data, we can compute the skill scores [Eq. (A5)] of the forecast datasets relative to the control. This approach allows us to not only evaluate the retrieved effective radii relative to the best-fit estimate, but it also enables us to evaluate the performance of the two different retrieval techniques relative to each other.

g. Applicability of the independent column approximation for radiative transfer

Because we use a plane-parallel, horizontally homogeneous radiative transfer model, we expect that our model will produce more accurate normalized cloud forcing values during overcast cases when the effects of horizontal photon transport are not significant. To estimate cloud fractional sky cover we use a technique developed by Long et al. (1999). They estimate cloud fraction using a relationship between cloud cover fraction and the difference between the estimated clear-sky and measured downwelling shortwave diffuse irradiances. In the current study we only consider periods when the cloud fractions of the warm boundary layer clouds exceed 0.90.

3. Using radiation to assess stratus cloud microphysical retrievals

To compare the effects of varying effective radii on downwelling shortwave irradiance at the surface we applied the RAPRAD radiative transfer model (section 2a) to 18 days of single layer, overcast, warm stratus clouds from January 1997 to January 1998 (five days in December, January and February; four days in March, April, and May; two days in June, July, and August; six days in September, October, and November). We identified the cases by visual inspection and obtained cloud layers and boundaries according to the procedure detailed in section 2b. Each of the selected case study periods has over a 90% instantaneous cloud cover as determined by the procedure in section 2g. Since the downwelling shortwave surface irradiance measurements had 1-min temporal resolution, we reduced the 10-s Atmospheric Remote Sensing of Clouds (ARSCL) data (Table 1) statistics and the 20-s microwave radiometer retrievals of cloud liquid water path to 1-min resolution. We used only those cases where, over the 60-s period under consideration, at least five of the six ARSCL-based cloud profiles had single-layer clouds. If at least 1 h of data for a day passed this test, we included the data for the particular day into our analysis. Our final stratus dataset consisted of over 80 h of data for a total of 5082 1-min samples over 18 days.

Using only single-layer, overcast cloud conditions was important to the study since we wanted to isolate the impact of cloud particle size while minimizing the impact of three-dimensional radiation transport effects. The mean and median cloud thickness were 987 and 833 m, respectively, while the standard deviation was 591 m. From the cloud thickness statistics cloud-top temperatures were generally much higher than the 253-K threshold as cloud bases were restricted to temperatures over 273 K. The cloud liquid water paths of the samples in the final pool of data had a mean of 0.120 mm, a mode of 0.050 mm, a median of 0.101 mm, and a standard deviation of 0.108 mm (Fig. 1b). Using a 4-yr dataset of 20-s liquid water paths (Fig. 1a), we find that both datasets have liquid water paths occurring below 0.02 mm. Note that liquid water path measurements from the microwave radiometer have a root-mean-square error of 0.02 mm (Liljegren et al. 2001). In spite of the uncertainties in small liquid water path measurements we use those cases where clouds are detected by the combined radar and lidar observations. Finally, the median is larger in the smaller 1-min liquid water path dataset (i.e., Fig. 1a), which is attributable to our selection of overcast cases only.

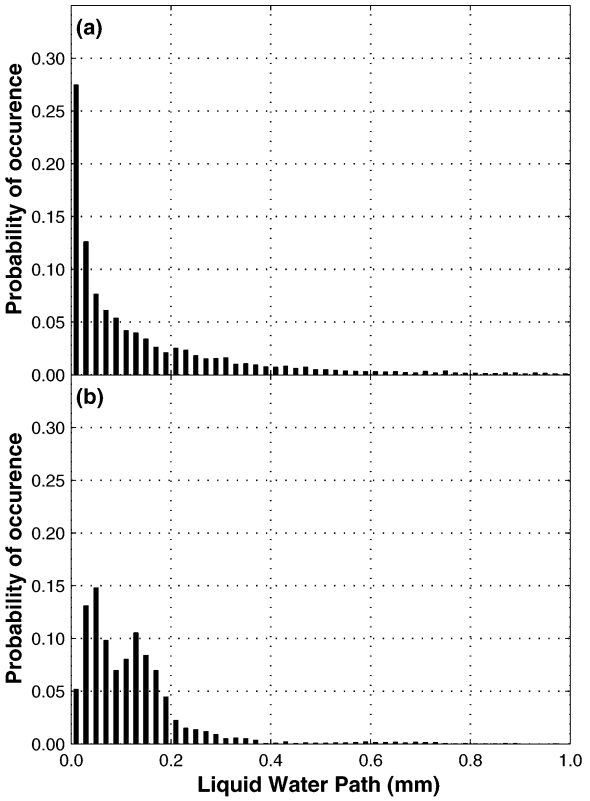

FIG. 1. Histogram of probability of occurrence of (a) 20-s LWP data for single-layer stratus clouds for the period 1997–2000 (367 760 samples) and (b) 1-min-averaged LWP data for 18 days having periods of overcast single-layer stratus clouds during the daytime (5082 samples). Histograms have a bin size of 0.02 mm.

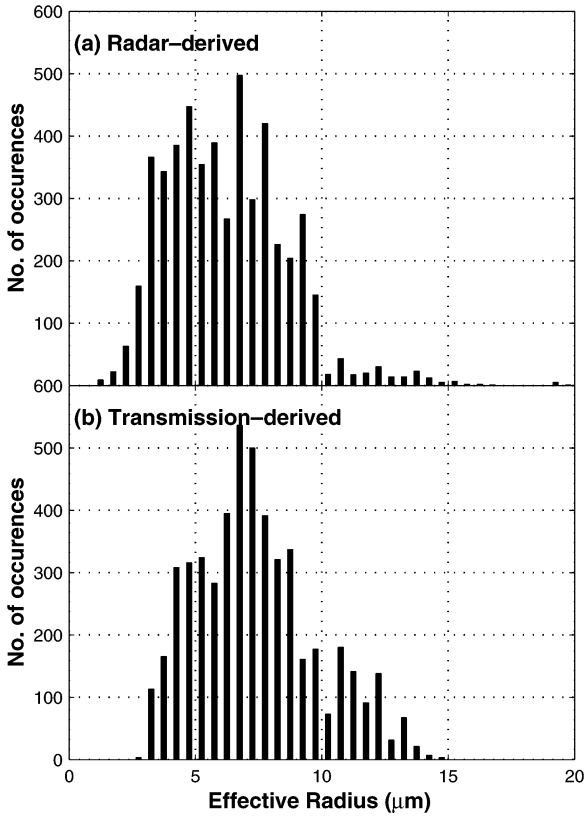

FIG. 2. Histograms of number of occurrences showing the effective radii distributions generated by the (a) radar- and (b) transmission-derived retrievals. The histograms have 5082 1-min-averaged points in bin sizes of 0.05 μm.

a. Cloud drop effective radius

Starting from the Miles et al. (2000) average effective radius of 5.4 μm, we iteratively reduce the difference across the whole dataset between modeled and observed normalized cloud forcing. The procedure involved radiative transfer calculations for all data points after manually selecting an effective radius that would reduce the difference across the whole dataset computed using the previous effective radius selection. Due to large computing expense we stopped the iteration when we reached a mean-square error of less than 2% (Table 4), as further iteration would have resulted in adjustments at a level of around 0.1 μm. The resulting best-fit effective radius was 7.5 μm.

The effective radii distributions obtained from the radar- and transmission-based retrieval techniques outlined in section 2d are illustrated in Fig. 2 and summarized in Table 2. Overall the transmission-derived effective radii have a mean of 7.38 μm, while the radar-derived effective radii have a mean of 6.33 μm. As the table and figure indicate, while the two sets of retrieved effective radii have similar distributions, there is a clear difference between their mean values with the radar-derived values being smaller. We also observed that there was no correlation between liquid water path and either the radar- or transmission-based effective radii implying that the clouds were probably nonadiabatic.

Independent sources, such as in situ aircraft measurements (Ackerman et al. 2003) from the Atmospheric Radiation Measurement Enhanced Shortwave Experiment II (ARESE II) and retrievals by Dong et al. (2000), corroborate a value of around 7.5 μm for a representative effective radius for stratus clouds at the SGP site. Note that our best-fit radius is a fixed value derived to reduce the cloud forcing bias in the whole dataset, unlike Dong et al. (2000) who compute effective radii sepa-

TABLE 2. Statistics of effective radii (μm) for 5082 1-min-averaged stratus cases.

Source of radii	Min radius	Max radius	Mean radius	Median radius	Std dev
Radar derived	1.41	19.69	6.23	6.01	2.36
Transmission derived	2.92	14.82	7.38	7.13	2.39

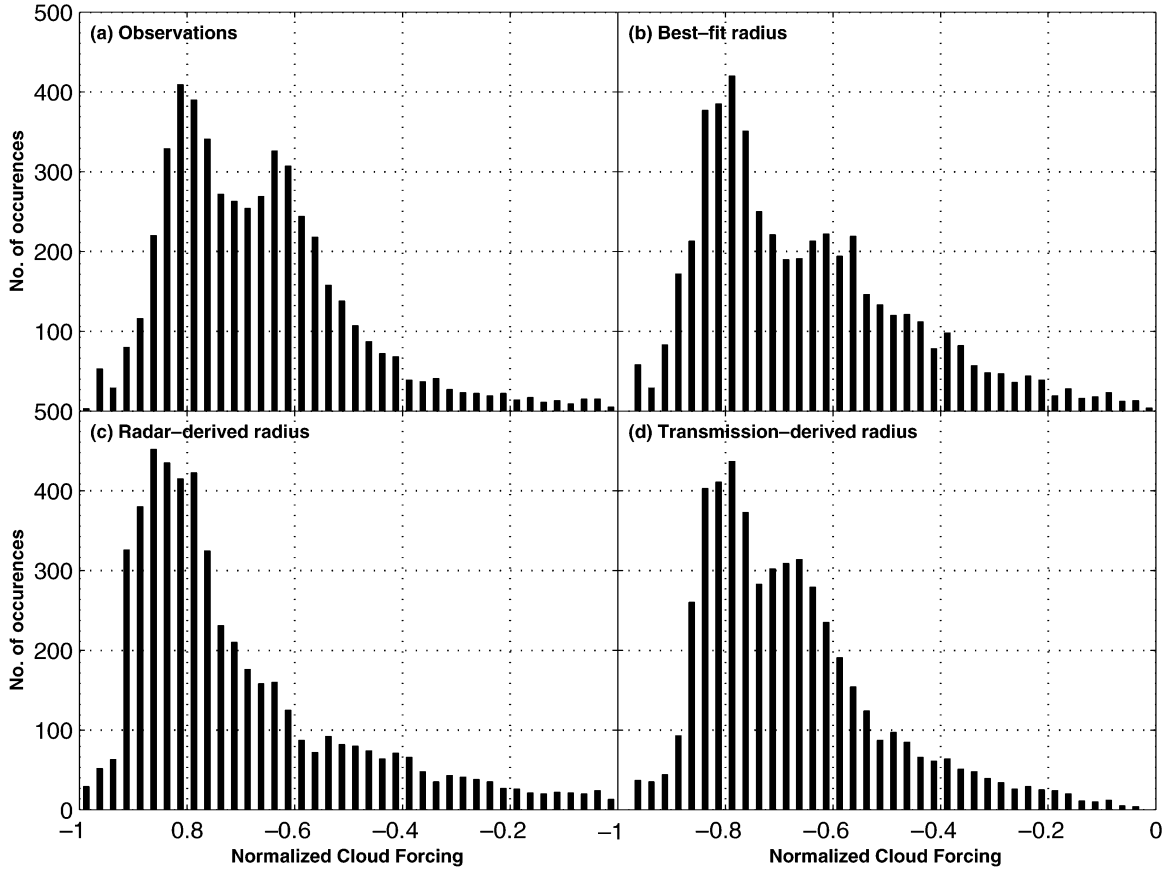

FIG. 3. Histograms of number of occurrences showing normalized cloud forcing for four different distributions. The best-fit effective radius is 7.5 μm.

rately for each individual case by matching observed transmission. The continental cloud average effective radius from Miles et al. (2000), however, is about 2 μm smaller than our best-fit radius. The continental stratus in the collection of Miles et al. (2000) have over 12% of cases with lower effective radii than our lowest transmission-derived effective radius of around 3 μm (Fig. 2b). Also, 25% of the cases in Miles et al. (2000) have effective radii less than 4 μm. Additionally, the Miles et al. (2000) study is a compilation of in situ observations from available literature and therefore has data from different locations and different investigators. Conditions at those sites, such as typical numbers of cloud condensation nuclei, may be quite different from the SGP site.

TABLE 3. Statistics of normalized cloud forcing for 5082 1-min-averaged warm boundary layer cloud data points.

Source of forcing	Mean forcing	Median forcing	Std dev
Best fit (7.5 μm)	−0.66	−0.70	0.19
Radar derived	−0.71	−0.78	0.20
Transmission derived	−0.68	−0.71	0.17
Observations	−0.67	−0.70	0.17

b. Comparison of modeled and observed normalized cloud forcing

Histograms of shortwave normalized cloud forcing for the observations and the model computations using retrieved cloud liquid water path and the three sets of cloud drop effective radii are illustrated in Fig. 3. The means, medians, and standard deviations for the points in these histograms are listed in Table 3. Scatterplots of the observed versus modeled normalized cloud forcing are presented in Fig. 4, together with the 1:1 lines. Applying the skill score methodology to these observations using the best-fit effective radius as the control produced the results listed in Table 4.

Inspecting Fig. 4 and Table 4, we find that the best-fit effective radius outperforms the radar-derived effective radii in explaining the observed normalized cloud forcings, and almost performs as well as the transmission-derived effective radii. For example, the observed normalized cloud forcing (Fig. 3a) is clearly bimodal and the transmission-derived results (Fig. 3d) capture this bimodality. While the best-fit effective radius forcings (Fig. 3b) do not capture the bimodality as well as the transmission-derived results, they are clearly better than those produced by the radar-derived effective radii

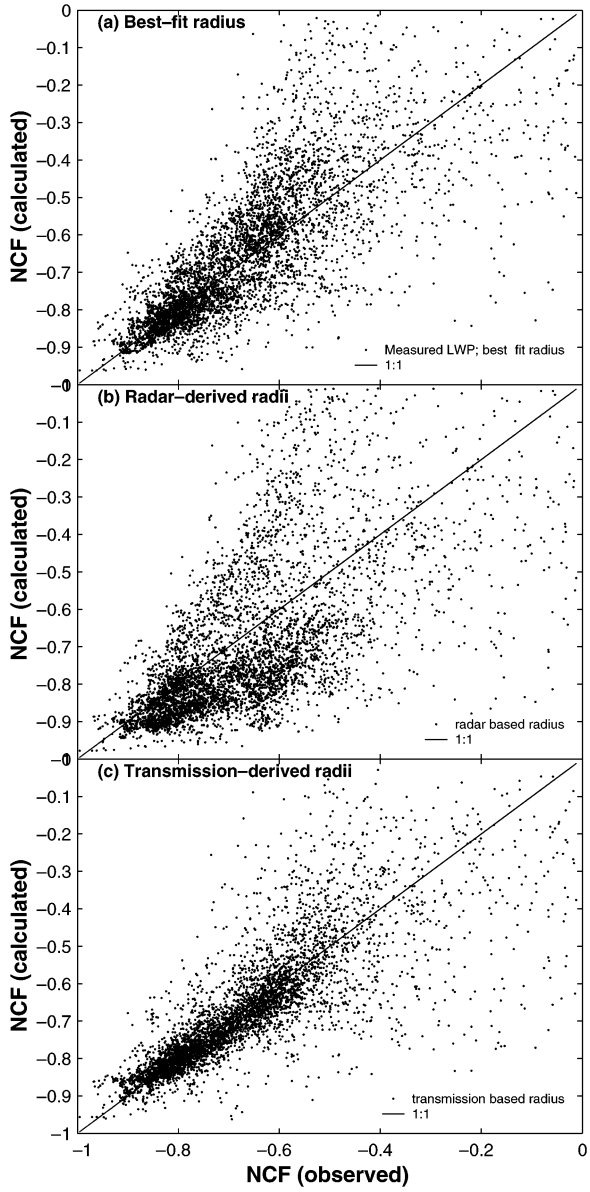

FIG. 4. Scatterplots of observed vs modeled cloud forcing using (a) a best-fit fixed effective radius of 7.5 μm, (b) radar-derived radii, and (c) transmission-derived radii.

(Fig. 3c). Considering the scatterplots, we find that the radar-derived normalized cloud forcing values are most biased relative to the observations. Furthermore, the primary improvement of the transmission-derived forcings over those based on the best-fit effective radius is a reduction in the random error relative to the observations (Table 4). Also, both the transmission-derived radii and best-fit effective radius results are comparable and highly correlated to the radiation observations (Table 4). Relative to the forcings based on the best-fit effective radius, the skill scores for the radar and transmission-derived effective radii forcings are −0.76 and 0.28, respectively. Because a positive skill score means improvement relative to the control and a negative value indicates degradation relative to the control, we conclude that in shortwave radiation studies the best-fit effective radius is preferable to the radar-derived effective radii of Kato et al. (2001) while the transmission-derived effective radii of Min and Harrison (1996) are preferable to the best-fit effective radius.

An observation that emerges from inspection of individual case study days is that the normalized cloud forcings based on the best-fit effective radius are consistently biased relative to the observations in one direction for extended intervals of time within a case study period. These biases are most likely the result of variations in stratus cloud drop effective radii within extended intervals of a case study period and from one case study period to the next. While the effects of inhomogeneities in cloud structure were not explicitly accounted for in either the transmission-derived effective radius retrievals or the normalized cloud forcing computations, we attempted to reduce their influence by selecting only overcast cases.

4. Stratus cloud radiative properties: Are drop sizes important?

The overall superior performance of the transmission-derived effective radii is not surprising as these radii are chosen to match the observed transmission in a visible solar band and we expect them to produce the most accurate downwelling shortwave irradiances at the surface. What we did find surprising was that the use of the best-fit effective radius produced skill scores almost as good as those using the transmission-derived effective radii. This result suggests that for computing surface radiation in warm clouds, explicit knowledge of

TABLE 4. The mean-square error in a comparison of 5082 observed and modeled cloud forcing data points is split into its components. The correlations between the three different modeled cloud forcings and observations are also shown along with the skill score for the radar- and transmission-derived forcings using climatological forcings as control.

Datasets compared	Correlation to observations	Mean-square error				Skill score
		Square of bias	Random error	Variance error	Total error	
Best fit	0.78	0.0003	0.0138	0.0007	0.0148	—
Radar derived	0.66	0.0014	0.0236	0.0008	0.0258	−0.76
Transmission derived	0.81	0.0000	0.0107	0.0000	0.0107	0.28

the liquid water paths for these clouds and a predetermined, fixed cloud particle size provides fairly accurate results.

a. The range of stratus cloud liquid water paths and effective radii

Both cloud liquid water path and cloud drop effective radius, the two important geophysical parameters for quantifying the microphysical and radiative properties of a stratus cloud, have natural limits dictated by nature, above and below which their values seldom occur. As a theoretical sensitivity study based on parameter values that never occur in nature is of little use, one must know the naturally occurring range for the two parameters. Therefore, we first consider the range of cloud liquid water paths and cloud drop effective radii that we expect to find in nature and then test the sensitivity of the surface normalized cloud forcing to realistic changes in their values.

In the current analysis we arrived at a value of 7.5 μm for the best-fit cloud drop effective radius, while the mean and standard deviation generated by the transmission-derived effective radius retrieval are 7.38 and 2.39 μm, respectively. The liquid water paths in our dataset have a mean of 0.120 mm, a standard deviation of 0.108 mm, and a median of 0.101 mm. For the radiative transfer calculations in this sensitivity study we set the cloud thickness to 500 m, which leads to a mean liquid water content of 0.2 g m^{-3} for a liquid water path of 0.1 mm. This value of the liquid water content is similar to the mean liquid water content of 0.18 g m^{-3} presented by Miles et al. (2000). We use a lognormal distribution with a lognormal width of 0.38 to characterize stratus cloud drop sizes after Miles et al. (2000).

b. Sensitivity of optical depth to changes in LWP and r_e

Using Eq. (3), together with the approximation that the extinction coefficient Q_{ext} of cloud drops is 2 at solar wavelengths, leads to the relation

$$\frac{\delta\tau}{\tau} = \frac{\delta\text{LWP}}{\text{LWP}} - \frac{\delta r_e}{r_e}. \tag{7}$$

Even though Eq. (7) shows that the liquid water path and effective radius are equally important in causing changes in the optical depth, and thereby changes in solar transmission and downwelling shortwave irradiance at the surface, we do not find strong evidence of their equal importance in our normalized cloud forcing study. The explanation for this finding lies in the fact that the downwelling shortwave irradiance at the surface is most sensitive to changes in optical depth for small values of the optical depth. Given the typical values of cloud drop effective radii that occur in stratus at the SGP site, the values of liquid water path that most often occur in stratus over the SGP site are sufficiently small and sufficiently varied to produce optical depths that fall across the range where the downwelling irradiance is most sensitive to changes in them. Changes in the magnitude of the cloud drop effective radius that occur naturally in continental clouds, however, are not sufficient to produce such large variations in the downwelling shortwave irradiance at the surface.

The ratio of the standard deviation to the mean for both liquid water path and effective radius provides a measure of how capable each of the two parameters are in influencing variations in optical depth. A ratio of 0.90 for the liquid water path compared to a value of 0.32 for effective radius shows that for typical SGP site values variability in liquid water path can influence optical depth 3 times as much as effective radius.

Looking at the issue from a different perspective we consider a stratus cloud with a liquid water path of 0.1 mm that contains drops with an effective radius of 8 μm. Using Eq. (7), we find that a 0.02-mm change in liquid water path, which is approximately 19% of the observed standard deviation of 0.108 mm, would need an opposing change of 1.6 μm in the effective radius, which is approximately 67% of the observed standard deviation of 2.39 μm, to keep the optical depth invariant. That is, small, unremarkable changes in typical stratus cloud liquid water path values will require relatively large, remarkable changes in effective radius to keep the optical depth invariant.

c. Sensitivity of cloud forcing to changes in LWP and r_e

While the previous section demonstrated that variations in liquid water path can influence the optical depth at least 3 times as much as the effective radius, the sensitivity might be different if we were to compare normalized cloud forcing, which would also include multiple scattering effects. To test this possibility we used RAPRAD (section 2a) to compute the downwelling irradiance at the surface for different stratus cloud liquid water paths and cloud drop size distributions confined to a 500-m cloud layer located from 0.5 to 1.0 km above ground level. The cloud drop size distributions were modeled with a lognormal distribution with a width of 0.38. We obtained the atmospheric thermodynamic state from the U.S. standard atmospheric profile and set the solar zenith angle to 60°. We computed the scattering and absorption coefficients, as well as the single-scattering albedo and asymmetry parameter of the drops, using Mie theory.

The normalized cloud forcings that resulted from our calculations, which are a function of effective radius and liquid water path, are shown in Fig. 5a. As the figure illustrates, the change in forcing is a nonlinear function of liquid water path with a larger magnitude slope, and hence sensitivity, at the lower values. In Fig. 5b we emphasize this nonlinearity by plotting the dependence of normalized cloud forcing versus liquid water path for a number of different cloud drop effective radii. As it

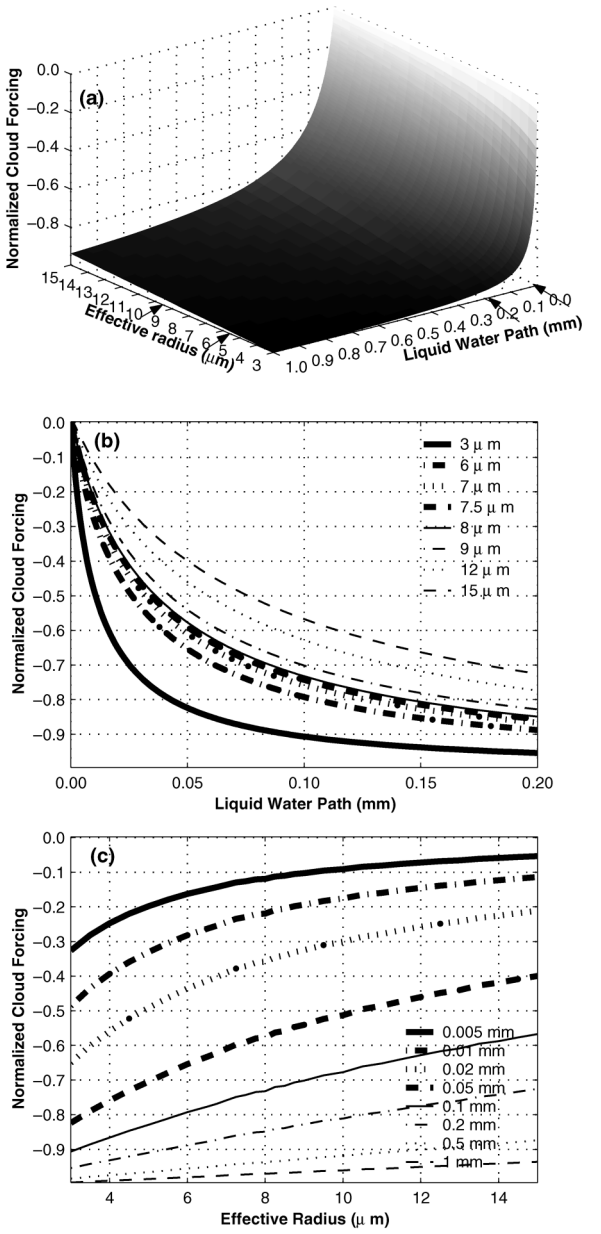

FIG. 5. Normalized cloud forcing calculated using our radiative transfer model, a plotted as function of (a) liquid water path and effective radius, (b) liquid water path for different fixed effective radii, and (c) effective radii for different fixed liquid water paths. The solar zenith angle used for the calculations is 60°. The arrows on the axes in (a) demarcate the observed ranges of cloud liquid water path and effective radius in the current dataset.

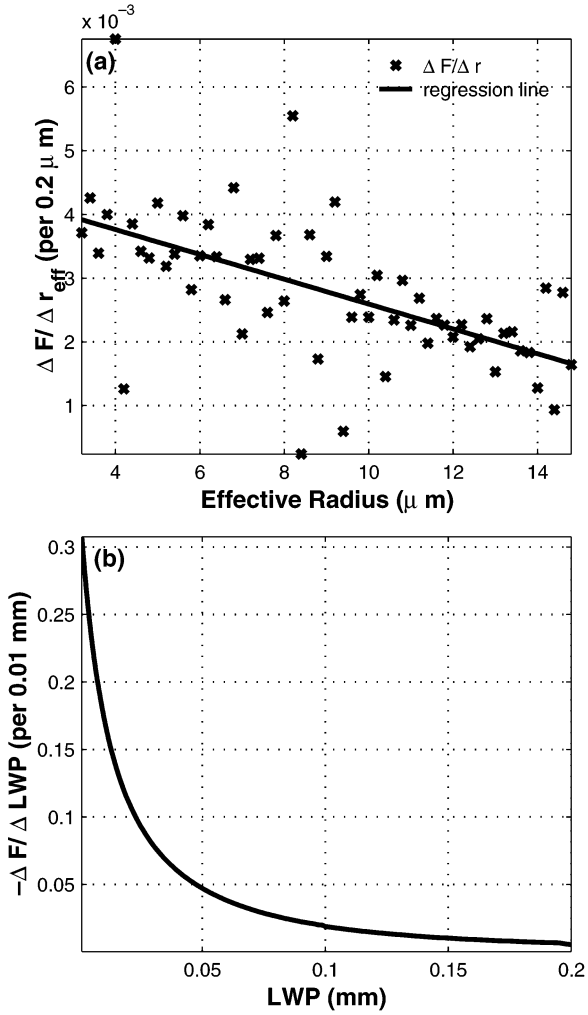

FIG. 6. The rate of change in normalized cloud forcing as a function of (a) effective radius (per 0.02-μm change in effective radius) for constant liquid water path of 0.1 mm and (b) liquid water path (per 0.01-mm change in liquid water path) for a constant effective radius of 7.5 μm.

turns out, at the SGP site most of the naturally occurring liquid water paths (Fig. 1) lie in the high-sensitivity region. The variation of forcing with effective radius is much more linear for typical values of cloud liquid water path (Fig. 5c) and hence much less sensitive to changes in cloud drop effective radius across the whole range of effective radii that we expect at the SGP site. The results presented here are not dependent on the width of the lognormal distribution that we use to represent the cloud drop size distribution. As Figs. 5a and 5b illustrate, the dominance of liquid water path in the determination of solar transmission is partly a result of the actual values of liquid water path and not solely due to higher variability of liquid water path when compared to the effective radius. This is evident from the nonlinearity of the curves in Figs. 5a and 5b, which show that variations in liquid water path below 0.2 mm will have a larger impact on surface radiation than values above that threshold.

To quantify the sensitivity of normalized cloud forcing to changes in cloud liquid water path and cloud drop effective radius, we computed the changes in normalized cloud forcing both as a function of cloud drop effective radius with the liquid water path held fixed at 0.1 mm (Fig. 6a) and as a function of cloud liquid water path

with the cloud drop effective radius held fixed at 7.5 μm (Fig. 6b). The scatter about the regression line in Fig. 6a is a result of the nonlinear variation of the extinction coefficient with wavelength and particle size that leads to abrupt variations in downwelling irradiance at the surface. The results in Fig. 6a illustrate how the rate of change of normalized cloud forcing varies from 0.001 to 0.006 per 0.2-μm change in drop size over the cloud drop effective radius range of 4–15 μm. This is much smaller than the 0.01–0.30 rate of change of normalized cloud forcing per 0.01-mm change in liquid water path over the range of typical values of cloud liquid water path (Fig. 6b). Note that both a 0.2-μm variation in effective radius and a 0.01-mm variation in liquid water path represent 5% of the observed variation in the two parameters, respectively.

Overall, the normalized cloud forcing is approximately 6 times more sensitive to changes in the liquid water path as it is to changes in the effective radius for typical values of these geophysical parameters for stratus cloud over the SGP site. In the previous section we showed that the liquid water path is 3 times as variable as effective radius. Factoring this into our analysis, we can conclude that uniform variation in both the parameters would still lead to a factor of 2 higher sensitivity of cloud forcing to variation in liquid water path, which is totally attributable to the regimes where each of the parameters actually occur. We conclude that liquid water path is the dominant parameter in correctly ascertaining solar transmission in continental stratus.

5. Conclusions

Our findings regarding the comparative sensitivity of solar radiation to variations in liquid water path and effective radius, the two most important geophysical parameters used to characterize the radiative impact of warm boundary layer clouds, lead us to conclude that accurate cloud liquid water paths are of absolute necessity in any climate model. Given that small liquid water path errors lead to large nonlinear errors in surface radiation, measures of the central tendency, such as the mean or median, and dispersion, like the standard deviation, must be accurately characterized in order to obtain reasonable surface shortwave fluxes. In comparison, errors in effective radius have a smaller impact on surface solar fluxes at a continental site such as the SGP.

In section 4b we noted that for a fixed optical depth a 19% uncertainty in liquid water path, a reasonable assumption given a root-mean-square error of 0.02 mm in microwave radiometer measurements, will lead to a corresponding uncertainty in effective radius equal to 67% of the observed standard deviation. We also noted in section 4c that over and above the impact of the higher variability in liquid water path, when compared to effective radius, cloud forcing, and hence solar transmission, it is 2 times as sensitive to liquid water variations compared to effective radius variations. The higher sensitivity of solar flux to liquid water path is a result of the regimes of natural occurrence of cloud liquid water paths and cloud drop effective radii.

Acknowledgments. We are grateful for the valuable comments and suggestions of the anonymous reviewers. This research was supported by the Office of Biological and Environmental Research of the U.S. Department of Energy under Contract DE-AC06-76RL01830 as part of the Atmospheric Radiation Measurement Program.

APPENDIX

Mean-Square Error and Skill Score

The mean-square error (mse) of a forecast is defined as

$$\mathrm{mse}_{f,o} = \frac{1}{N}\sum_{i=1}^{N}(F_i - O_i)^2, \tag{A1}$$

with N being the number of observations and F and O denoting the forecast and observation data, respectively. The correlation coefficient between the forecast and observations using the same notation can be written as

$$R_{f,o} = \frac{\overbrace{\frac{1}{N}\sum_{i=1}^{N}[(F_i - \overline{F}) \times (O_i - \overline{O})]}^{\mathrm{cov}_{f,o}}}{\underbrace{\sqrt{\frac{1}{N}\sum_{i=1}^{N}(F_i - \overline{F})^2}}_{\sigma_f}\ \underbrace{\sqrt{\frac{1}{N}\sum_{i=1}^{N}(O_i - \overline{O})^2}}_{\sigma_o}}, \tag{A2}$$

where $\overline{F}$ and $\overline{O}$ are the means of the forecast and observed data, respectively. As seen from Eq. (A2), the correlation coefficient can also be represented as

$$R_{f,o} = \mathrm{cov}_{f,o}(\sigma_f\sigma_o)^{-1}, \tag{A3}$$

where $\mathrm{cov}_{f,o}$ is the covariance of the forecast and observations and σ_f and σ_o the standard deviations of the forecast and observations, respectively. Expansion of Eq. (A1) and use of Eq. (A3) gives us

$$\mathrm{mse}_{f,o} = \underbrace{(\overline{F} - \overline{O})^2}_{\mathrm{bias}^2} + \underbrace{(1 - R_{f,o})(\sigma_f^2 + \sigma_o^2)}_{\text{random error}} + \underbrace{R_{f,o}(\sigma_f - \sigma_o)}_{\text{variance error}}, \tag{A4}$$

where the three terms are useful in determining the sources of error.

Having defined the mean error in terms of the forecast and observed variables, we need to determine whether our forecast has any skill given that we have a value for $\mathrm{mse}_{f,o}$. This comparison is done with a control that

is generally a climatological value. The skill score is then defined as

$$SS = \frac{(mse_{f,o} - mse_{c,o})}{(0 - mse_{c,o})} = 1 - \frac{mse_{f,o}}{mse_{c,o}}, \quad (A5)$$

where $mse_{c,o}$ is the mean-square error of the control when compared to the observations, As can be seen from Eq. (A5), a positive value reflects skill in the forecast. Negative values imply that our forecast is worse than the climatological value implying the need for improvement.

REFERENCES

Ackerman, T. P., M. Sengupta, and E. E. Clothiaux, cited 1999: A paradigm for testing cloud parameterizations. *Extended Abstracts, Ninth ARM Science Team Meeting,* San Antonio, TX, DOE Atmospheric Radiation Measurement Program, 9 pp. [Available online at http://www.arm.gov/docs/documents/technical/conf_9903/ackerman-99.pdf.]

——, D. M. Powell, and R. T. Marchand, 2003: Quantifying the magnitude of anomalous solar absorption. *J. Geophys. Res.,* **108,** 4273, doi:10.1029/2002JD002674.

Albrecht, B. A., C. S. Bretherton, D. Johnson, W. H. Schubert, and A. S. Frisch, 1995: The Atlantic Stratocumulus Transition Experiment—ASTEX. *Bull. Amer. Meteor. Soc.,* **76,** 889–904.

Angstrom, A., 1929: On the transmission of sun radiation and on dust in air. *Geogr. Ann.,* **2,** 156–166.

Berk, A., L. S. Bernstein, and D. C. Robertson, 1989: MODTRAN: A moderate resolution model for LOWTRAN 7. AFGL Tech. Rep. GL-TR-89-0122, AFGL, 38 pp. [Available from Geophysics Directorate/GPOS, 29 Randolph Rd., Hanscom AFB, MA 01731-3010.]

Charlock, T. P., F. G. Rose, and D. A. Rutan, 2001: Aerosols and the residual clear-sky insolation discrepancy. *Extended Abstracts, 11th ARM Science Team Meeting,* Atlanta, GA, DOE Atmospheric Radiation Measurement Program, 15 pp. [Available online at http://www.arm.gov/docs/documents/technical/conf_0103/charlock-tp.pdf.]

Charlson, R. J., J. E. Lovelock, M. O. Andrae, and S. G. Warren, 1987: Oceanic phytoplankton, atmospheric sulfur, cloud albedo and climate. *Nature,* **326,** 655–661.

Chen, C. T., and V. Ramaswamy, 1996: Sensitivity of simulated global climate to perturbations in low-cloud microphysical properties. Part I: Global uniform perturbations. *J. Climate,* **9,** 1385–1402.

Clothiaux, E. E., T. P. Ackerman, G. G. Mace, K. P. Moran, R. T. Marchand, M. A. Miller, and B. E. Martner, 2000: Objective determination of cloud heights and radar reflectivities using a combination of active remote sensors at the ARM CART sites. *J. Appl. Meteor.,* **39,** 645–665.

d'Almeida, G. A., P. Koepke, and E. P. Shettle, 1991: *Atmospheric Aerosols: Global Climatology and Radiative Characteristics.* A. Deepak Publishing, 561 pp.

Del Genio, A. D., and A. B. Wolf, 2000: The temperature dependence of liquid water path of low clouds at the southern Great Plains. *J. Climate,* **13,** 3465–3486.

Dong, X., P. Minnis, T. P. Ackerman, E. E. Clothiaux, G. G. Mace, C. N. Long, and J. C. Liljegren, 2000: A 25-month database of stratus cloud properties generated from ground-based measurements at the Atmospheric Radiation Measurement Southern Great Plains site. *J. Geophys. Res.,* **105,** 4529–4537.

Duda, D. P., G. L. Stephens, and S. K. Cox, 1991: Microphysical and radiative properties of marine stratocumulus from tethered balloon measurements. *J. Appl. Meteor.,* **30,** 170–186.

Flatau, P. J., G. J. Tripoli, J. Verlinde, and W. R. Cotton, 1989: The CSU-RAMS cloud microphysics module: General theory and code documentation. Colorado State University Tech. Rep. 451, Fort Collins, CO, 88 pp.

Han, Q., W. B. Rossow, and A. Lacis, 1994: Near global survey of effective droplet radii in liquid water cloud using ISCCP data. *J. Climate,* **7,** 465–497.

Hansen, J. E., and L. D. Travis, 1974: Light scattering in planetary atmospheres. *Space Sci. Rev.,* **16,** 527–610.

Harrison, L., J. Michalsky, and J. Berndt, 1994: Automated multifilter rotating shadow-band radiometer: An instrument for optical depth and radiation measurements. *Appl. Opt.,* **22,** 5118–5125.

Hartmann, D. L., M. E. Ockert-Bell, and M. L. Michelsen, 1992: The effect of cloud type on earth's energy balance: Global analysis. *J. Climate,* **5,** 1281–1304.

Heymsfield, A. J., 1993: Microphysical structures of stratiform and cirrus clouds. *Aerosol–Cloud–Climate Interactions,* P. V. Hobbs, Ed., Academic Press, 97–119.

Hobbs, P. V., 1993: Aerosol–cloud interactions. *Aerosol–Cloud–Climate Interactions,* P. V. Hobbs, Ed., Academic Press, 33–73.

Hu, Y. X., and K. Stamnes, 1993: An accurate parameterization of the radiative properties of water clouds suitable for use in climate models. *J. Climate,* **6,** 728–742.

Kato, S., T. P. Ackerman, E. E. Clothiaux, J. H. Mather, G. G. Mace, M. L. Wesely, F. Murcray, and J. Michalsky, 1997: Uncertainties in modeled and measured clear-sky surface shortwave irradiances. *J. Geophys. Res.,* **102,** 25 881–25 898.

——, ——, E. G. Dutton, N. Laulainen, and N. Larson, 1999a: A comparison of modeled and measured shortwave irradiance for a molecular atmosphere. *J. Quant. Spectrosc. Radiat. Transfer,* **61,** 493–502.

——, ——, J. H. Mather, and E. E. Clothiaux, 1999b: The *k*-distribution method and correlated-*k* approximation for a shortwave radiative transfer model. *J. Quant. Spectrosc. Radiat. Transfer,* **62,** 109–121.

——, G. G. Mace, E. E. Clothiaux, and J. C. Liljegren, 2001: Doppler cloud radar derived drop size distributions in liquid water stratus clouds. *J. Atmos. Sci.,* **58,** 2895–2911.

Liljegren, J. C., 1994: Two-channel microwave radiometer for observations of total column precipitable water vapor and cloud liquid water path. Preprints, *Fifth Symp. on Global Change Studies,* Nashville, TN, Amer. Meteor. Soc., 262–269.

——, E. E. Clothiaux, G. G. Mace, S. Kato, and X. Dong, 2001: A new retrieval for cloud liquid water path using a ground-based microwave radiometer and measurements of cloud temperature. *J. Geophys. Res.,* **106,** 14 485–14 500.

Long, C. N., and T. P. Ackerman, 2000: Identification of clear skies from broadband pyranometer measurements and calculation of downwelling shortwave cloud effects. *J. Geophys. Res.,* **105,** 15 609–15 626.

——, ——, and J. J. Deluisi, 1999: Estimation of fractional sky cover from broadband SW radiometer measurements. Preprints, *10th Conf. on Atmospheric Radiation,* Madison, WI, Amer. Meteor. Soc., 383–386.

——, K. Younkin, and D. M. Powell, cited 2001: Analysis of the Dutton et al. IR loss correction technique applied to ARM diffuse SW measurements. *Extended Abstracts, 11th ARM Science Team Meeting,* Atlanta, GA, DOE Atmospheric Radiation Measurement Program, 9 pp. [Available online at http://www.arm.gov/docs/documents/technical/conf_0103/long-cn.pdf.]

Martin, G. M., D. W. Johnson, and A. Spice, 1994: The measurement and parameterization of effective radius of drops in warm stratocumulus clouds. *J. Atmos. Sci.,* **51,** 1823–1842.

Michalsky, J. J., J. A. Schlemmer, W. E. Berkhaiser, J. L. Berndt, L. C. Harrison, N. S. Laulainen, N. R. Larson, and J. C. Barnard, 2001: Multilayer measurements of aerosol optical depth in the Atmospheric Radiation Measurement and Quantitative Links programs. *J. Geophys. Res.,* **106,** 12 099–12 107.

Miles, N. L., J. Verlinde, and E. E. Clothiaux, 2000: Cloud droplet size distributions in low-level stratiform clouds. *J. Atmos. Sci.,* **57,** 295–311.

Min, Q., and L. C. Harrison, 1996: Cloud properties derived from

surface MFRSR measurements and comparison with GOES results at the ARM SGP site. *Geophys. Res. Lett.*, **23,** 1641–1644.
Noonkester, V. R., 1984: Droplet spectra observed in marine stratus cloud layers. *J. Atmos. Sci.,* **41,** 829–845.
Pruppacher, H. R., and J. D. Klett, 1997: Microstructure of atmospheric clouds and precipitation. *Microphysics of Clouds and Precipitation,* R. D. Rosen Ed., Kluwer Academic, 10–29.
Ramaswamy, V., and C. T. Chen, 1993: An investigation of the global solar radiative forcing due to changes in the cloud liquid water path. *J. Geophys. Res.,* **98,** 16 703–16 712.
Schmit, T. J., W. F. Feltz, W. P. Menzel, J. Jung, A. P. Noel, J. N. Heil, J. P. Nelson III, and G. S. Wade, 2002: Validation and use of GOES sounder moisture information. *Wea. Forecasting,* **17,** 139–154.
Stephens, G. L., 1978: Radiation profiles in extended water clouds. I: Theory. *J. Atmos. Sci.,* **35,** 2111–2122.
——, G. W. Paltridge, and C. M. R. Platt, 1978: Radiation profiles in extended water clouds. III: Observations. *J. Atmos. Sci.,* **35,** 2133–2141.
Szczodrak, M., P. H. Austin, and P. B. Krummel, 2001: Variability of optical depth and effective radius in marine stratocumulus. *J. Atmos. Sci.,* **58,** 2912–2926.
Toon, O. B., and T. P. Ackerman, 1981: Algorithms for the calculation of scattering by stratified spheres. *Appl. Opt.,* **20,** 3657–3660.
——, C. P. McKay, and T. P. Ackerman, 1989: Rapid calculation of radiative heating rates and photodissociation rates in inhomogeneous multiple scattering atmospheres. *J. Geophys. Res.,* **94,** 16 287–16 301.
Westwater, E. R., 1993: Ground-based microwave remote sensing of meteorological variables. *Atmospheric Remote Sensing by Microwave Radiometry,* M. A. Jannsen, Ed., John Wiley and Sons, 145–213.